GeoScienceWorld
Lithosphere
Volume 2021, Article ID 3341849, 13 pages
https://doi.org/10.2113/2021/3341849

Lithosphere

*Research Article*

# Elastic-Electrical Rock-Physics Template for the Characterization of Tight-Oil Reservoir Rocks

**Mengqiang Pang**,[1] **Jing Ba**,[1] **José M. Carcione**,[1,2] **and Erik H. Saenger**[3,4,5]

[1]*School of Earth Sciences and Engineering, Hohai University, Nanjing 211100, China*
[2]*National Institute of Oceanography and Applied Geophysics (OGS), Trieste, Italy*
[3]*Hochschule Bochum, Am Hochschulcampus 1, D-44801 Bochum, Germany*
[4]*Fraunhofer IEG (Institution for Energy Infrastructures and Geothermal Energy), Am Hochschulcampus 1, 44801 Bochum, Germany*
[5]*Institute of Geology, Mineralogy, and Geophysics, Ruhr-University Bochum, Universitätsstrasse 150, 44801 Bochum, Germany*

Correspondence should be addressed to Jing Ba; jba@hhu.edu.cn

Received 5 February 2021; Accepted 22 May 2021; Published 5 July 2021

Academic Editor: Steve Banham

Copyright © 2021 Mengqiang Pang et al. Exclusive Licensee GeoScienceWorld. Distributed under a Creative Commons Attribution License (CC BY 4.0).

Tight-oil reservoirs have low porosity and permeability, with microcracks, high clay content, and a complex structure resulting in strong heterogeneities and poor connectivity. Thus, it is a challenge to characterize this type of reservoir with a single geophysical methodology. We propose a dual-porosity-clay parallel network to establish an electrical model and the Hashin-Shtrikman and differential effective medium equations to model the elastic properties. Using these two models, we compute the rock properties as a function of saturation, clay content, and total and microcrack porosities. Moreover, a 3D elastic-electrical template, based on resistivity, acoustic impedance, and Poisson's ratio, is built. Well-log data is used to calibrate the template. We collect rock samples and log data (from two wells) from the Songliao Basin (China) and analyze their microstructures by scanning electron microscopy. Then, we study the effects of porosity and clay content on the elastic and electrical properties and obtain a good agreement between the predictions, log interpretation, and actual production reports.

## 1. Introduction

Tight-oil reservoirs are widely distributed around the world (e.g., [1, 2]) and become a new prospect of hydrocarbon exploration and development [3, 4]. Compared with conventional reservoirs, tight-oil rocks exhibit low porosity and permeability, a complex pore structure, and higher clay content [5–7]. Theoretical and experimental studies have shown that their permeability depends on microcracks [8–11], which significantly affect fluid flow [12–15] and the elastic properties [16–18]. In particular, recent works analyzed the effect of clay minerals, which fill the pore space and block the hydrocarbon migration [19–21], on the rock properties [22–24], such as density, and bulk and shear moduli.

Many studies have been performed on the pore structure and mineral composition of tight-oil rocks [25–29]. In particular, Sun et al. [6] established a pore-network model by using 3D digital cores to simulate the influences of the size, length, and inclination of microcracks. Yan et al. [4] studied physical properties, such as porosity, permeability, pore structure, and wettability, on samples with different saturations, based on nuclear magnetic resonance and imbibition methods. Tan et al. [29] analyzed the tight-oil rock characteristics by utilizing scanning electron microscopic (SEM) and ultrasonic experiments on core samples to construct a brittleness model. By using a single-scattering model and the spectral-ratio method, Ma and Ba [28] estimated the coda and intrinsic attenuation of tight-oil siltstones and analyzed the effects of saturation, pore structure, and mineral content on wave attenuation. In geophysical exploration, the evaluations of tight-oil reservoirs are mainly based on acoustic/elastic data. However, the use of a single technique cannot be enough to characterize these reservoirs [30], and seismic-electromagnetic methods are increasingly applied [31–37].

Several experimental and theoretical studies have been performed to analyze the relationship between the elastic and electrical properties of porous rocks [31, 38–40].

Downloaded from http://pubs.geoscienceworld.org/gsa/lithosphere/article-pdf/doi/10.2113/2021/3341849/5355757/3341849.pdf
by OGS Inst Naz Oceanografia Geofisica Sperim - Biblioteca user

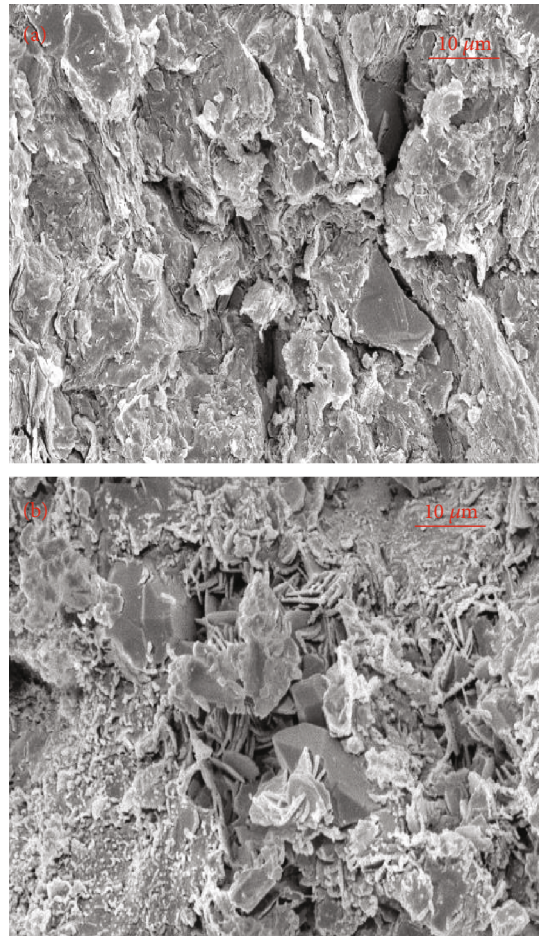


Figure 1: SEM photographs showing (a) intergranular pores and microcracks and (b) clay minerals (illite).

Kazatchenko et al. [41] proposed a modeling technique by combining electrical conductivity and acoustic wave velocity. Han et al. [42] collected 63 clean or high muddy sandstones and performed a set of experiments under different confining pressures, to analyze the elastic-electrical properties as a function of porosity, permeability, and clay content. Jensen et al. [37] related elastic and electric attributes by using differential effective medium (DEM) theories. He calibrated this approach with core samples and well-log data. Based on laboratory measurements on carbonate samples, Cilli and Chapman [32] used a power-law relation between porosity and pore aspect ratio to analyze the effects of porosity on resistivity and elastic moduli.

Recent works have showed that the clay minerals significantly reduce rock resistivity [43–46]. Dewitte [47] considered clay minerals as a liquid and assumed a parallel network of water and clay to estimate conductivity, while Aguilera and Aguilera [48] proposed a dual-porosity model (matrix and microcracks), to obtain the electrical properties of fractured reservoirs.

Here, we establish a dual-porosity-clay electrical model, where clay is connected to pores and microcracks in parallel. The Hashin and Shtrikman [49] (HS) equation is used to compute the elastic moduli of the nonconductive mineral mixture and the differential effective medium (DEM) theory [50] to add pores, microcracks, and clay minerals into the solid mixture. Finally, the Gassmann equation [51] yields the elastic modulus of the saturated rock. These models allow us to analyze how the elastic and electrical properties are affected by water saturation, total and microcrack porosities, and clay content. By combining the two models, a 3D elastic-electrical template is built, and data from core samples and logging curves from two wells of the Songliao Basin are used. The results are then compared with the log interpretation and actual production reports.

## 2. Reservoir Characteristics

The reservoirs are located within the Qingshankou Formation in the G area of Songliao Basin, China, which has developed high-quality source rocks with a broad-range distribution and good continuity [52]. The target formation shows high oil saturation, light-oil characteristics, low ratio of movable water, and a thickness of 70-110 m. The pore-pressure range is 22-32 MPa, and the temperature is around 80°C [27]. The porosity range is 4%-15%, with an average of 8.5%, and the permeability ranges from 0.01 mD to 0.5 mD. The lithology of the reservoirs is dominated by tight siltstones with high clay content.

Downloaded from http://pubs.geoscienceworld.org/gsa/lithosphere/article-pdf/doi/10.2113/2021/3341849/5355757/3341849.pdf
by OGS Inst Naz Oceanografia Geofisica Sperim - Biblioteca user

Table 1: Physical properties of the samples.

| Sample | A | B | C | D | E | F | G | H | I | J | K | L |
|---|---|---|---|---|---|---|---|---|---|---|---|---|
| Porosity (%) | 2.88 | 4.60 | 5.20 | 5.56 | 5.60 | 5.79 | 5.80 | 6.45 | 10.87 | 12.75 | 13.09 | 13.97 |
| Dry rock density (g/cm$^3$) | 2.61 | 2.56 | 2.58 | 2.53 | 2.52 | 2.41 | 2.55 | 2.38 | 2.29 | 2.3 | 2.28 | 2.26 |
| Clay content (%) | 2.8 | 8.2 | 1.9 | 12.5 | 2.4 | 3.9 | 3 | 5.5 | 5.5 | 4.4 | 5.5 | 5.5 |

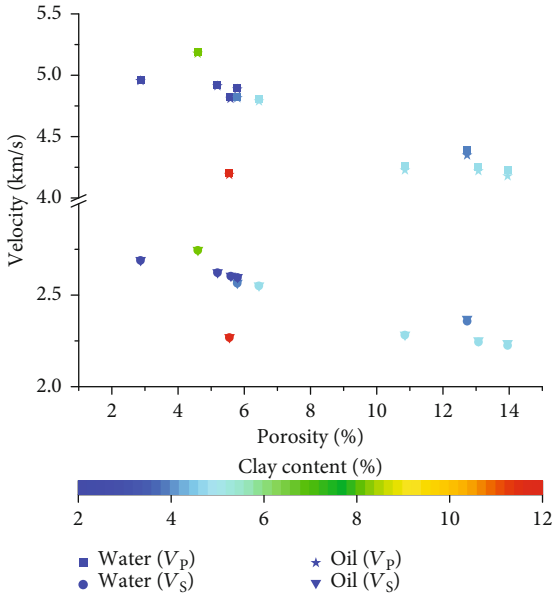


Figure 2: Elastic wave velocities of the samples as a function of porosity. The color bar indicates clay content.

The SEM results of core samples are shown in Figure 1. The reservoir storage space mainly includes intergranular and dissolved pores, with clay minerals, mostly illite. The nonconductive minerals (excluding clay) are quartz, feldspar, and small amounts of dolomite and calcite.

We have collected 12 tight-oil rock specimens and performed ultrasonic experiments at in situ conditions (80°C, confining pressure of 50 MPa, and pore pressure of 25 MPa). The samples are collected at a depth of 2200 m (cylinders of 25 mm in diameter and 50-56 mm in length), whose physical properties are given in Table 1. The acoustic wave velocities of oil (kerosene)-saturated and water-saturated states are measured at a frequency of 1 MHz [25, 28]. The results are given in Figure 2, showing the velocities as a function of porosity at full water/oil saturation, where the color bar represents clay content. The velocities decrease with increasing clay content and porosity. The P-wave velocities of the oil- and water-saturated samples are similar when the porosity is small. However, they tend to differ as porosity increases. The S-wave velocity is similar in the two cases.

The reservoir resistivity, porosity, and natural gamma values of Well A are obtained from log data. Clay content is determined from the gamma-ray log (see Appendix A). Figure 3 shows the resistivity as a function of clay content and porosity. The rocks have a high clay content, which ranges between 5% and 30%, and the porosity from 5% to

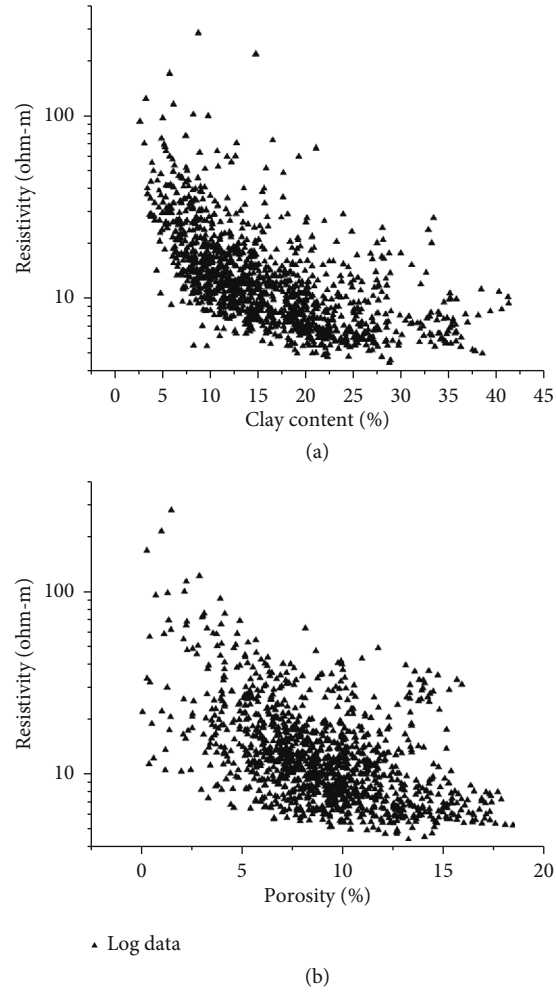


Figure 3: Electrical resistivity at Well A as a function of clay content (a) and porosity (b).

15%. The resistivity decreases with increasing clay content and porosity.

## 3. Rock-Physics Models

*3.1. Elastic Model.* Figure 4 shows the flowchart of the elastic-electrical model. First, we obtain the properties of the mineral mixture with the HS equation (see Appendix B). The stiff pores and soft microcracks are assumed to be spherical and oblate, with aspect ratios of 1 and 0.002, respectively. Then, the DEM theory (Appendix B) is used to add pores and microcracks into the mineral mixture and obtain the properties of the rock frame. Moreover, by using the DEM equation,

Downloaded from http://pubs.geoscienceworld.org/gsa/lithosphere/article-pdf/doi/10.2113/2021/3341849/5355757/3341849.pdf
by OGS Inst Naz Oceanografia Geofisica Sperim - Biblioteca user

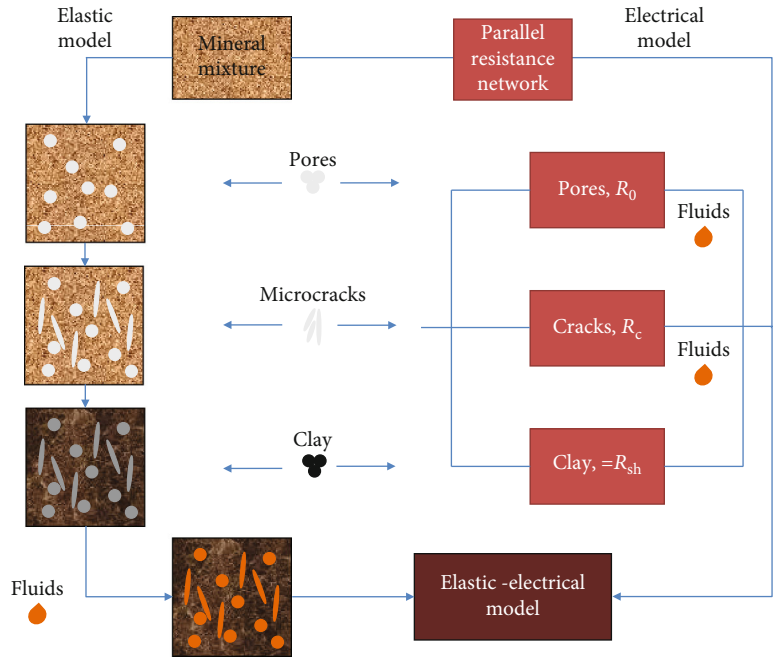


FIGURE 4: Flowchart of the elastic-electrical model.

clay minerals are added to the frame (with an aspect ratio of 0.1).

The fluid properties are reservoir pressure/temperature conditions which are obtained with the equations of Batzle and Wang [53], and an approximate method (see Appendix B) is used to estimate the effective bulk modulus of the fluid mixture [54, 55]. Finally, the Gassmann equation yields the properties of the wet rock.

*3.2. Electrical Model.* Archie [56] assumed a rock without clay and other conductive minerals, so that the rock conductivity only depends on the formation water in the pore space. The Archie equation for sandstone containing only intergranular pores is

$$F = \frac{R_0}{R_w} = \frac{a}{\phi^m}, \qquad I = \frac{b}{S_w^{\ n}}, \tag{1}$$

where $F$ is the formation factor; $\phi$ is the porosity; $m$ is the porosity exponent; $R_0$ is the rock resistivity; $R_w$ is the resistivity of brine (water); $I$ is the resistivity index, a function of brine saturation, $S_w$; $a$ and $b$ are lithology coefficients; and $n$ is the saturation exponent.

The complex pore structure of reservoir rocks restricts the application of the Archie equation and affects the estimation of the hydrocarbon saturation. Aguilera and Aguilera [48] proposed a dual-porosity model, where the pore-containing matrix is paralleled with the microcracks, to obtain the electrical resistivity (see Appendix C). However, this model does not consider the clay content, which significantly decreases the resistivity (2-6 ohm-m, see [40, 45]). We then add the effects of clay and develop a dual-porosity-clay (DPCL) parallel network model, as is shown in Figure 4. The total resistivity $R_t$ is

$$\frac{1}{R_t} = \frac{1-\phi_c - V_{sh}}{R_0} + \frac{\phi_c}{R_c} + \frac{V_{sh}}{R_{sh}}, \tag{2}$$

where $R_0$ is the resistivity of the frame (with intergranular pores); $\phi_c$ is the microcrack porosity; $R_c$ is the resistivity of the microcracks, which equals $R_w$ when the water saturation is 1 ([48]); $V_{sh}$ is the clay content; and $R_{sh}$ is the resistivity of the clay minerals.

It is

$$R_t = \frac{R_0 R_c R_{sh}}{R_c R_{sh}(1-\phi_c - V_{sh}) + R_0 R_{sh}\phi_c + R_0 R_c V_{sh}}, \tag{3}$$

according to the Archie equation,

$$R_0 = a\phi_0^{-m_0} b S_W^{-n} R_w, \qquad R_c = b S_W^{-n} R_w, \tag{4}$$

where $\phi_0$ is the matrix porosity, $\phi_0 = (\phi - \phi_c)/V_0$, where the volume ratio of the matrix is $V_0 = 1 - \phi_c - V_{sh}$, and $m_0$ is the matrix porosity exponent.

## 4. Model Response and Data

*4.1. Electrical Response.* In order to verify the DPCL model, a specific case is considered to predict the resistivity. The results are compared with the dual-porosity model and the clay-bearing electrical equation by Sava & Hardage [57],

Downloaded from http://pubs.geoscienceworld.org/gsa/lithosphere/article-pdf/doi/10.2113/2021/3341849/5355757/3341849.pdf
by OGS Inst Naz Oceanografia Geofisica Sperim - Biblioteca user

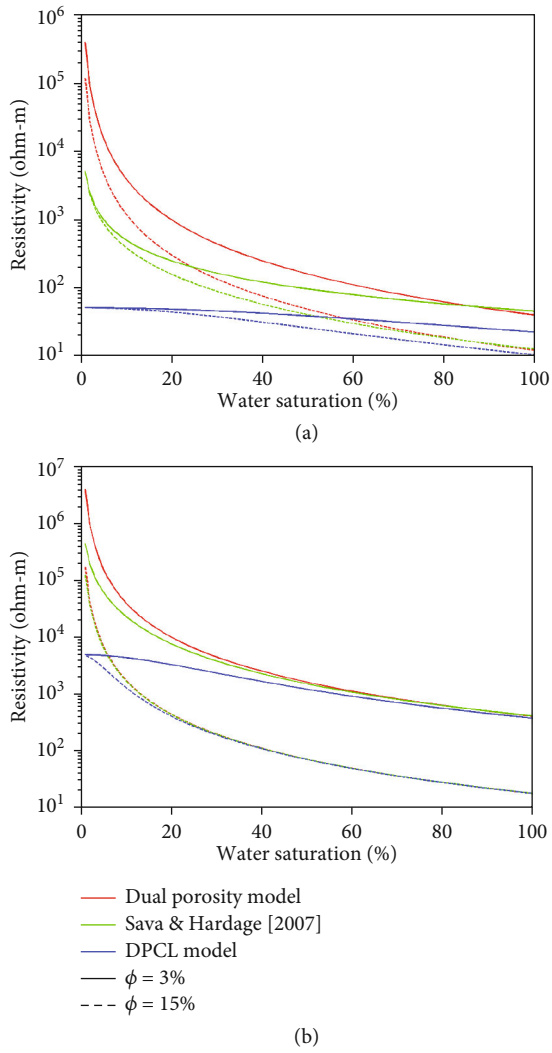


FIGURE 5: Resistivity as a function of water saturation: (a) high microcrack porosity (1%) and clay content (10%); (b) low microcrack porosity (0.01%) and clay content (0.1%).

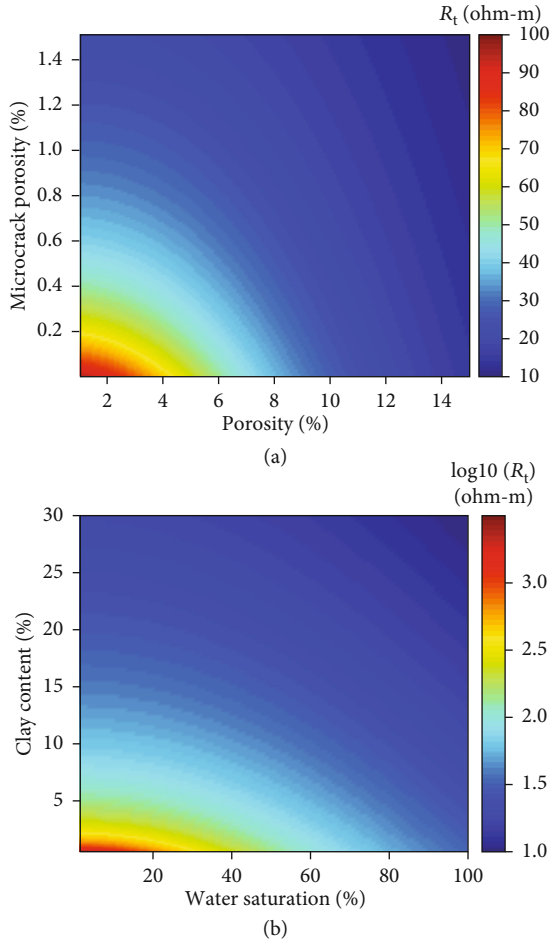


FIGURE 6: Resistivity as a function of (a) total and microcrack porosities and (b) water saturation and clay content.

which are given in Appendix C. The rock parameters are: $a = b = 1$, $m_0 = m = n = 2$, the resistivity of clay is 5 ohm-m, and the resistivity of brine is 0.41 ohm-m (according to [58]). Figure 5 shows the resistivity estimated with the three models as a function of water saturation at two total porosities (3% and 15%), microcrack porosities (1% and 0.01%), and clay contents (10% and 0.1%). The resistivity decreases when these quantities increase, with that of the DPCL model significantly smaller, compared to the other two models, when the microcrack porosity and clay content are high (Figure 5(a)). In Figure 5(b), as the microcrack porosity and clay content decrease, the difference among the results of the three models becomes smaller, approaching zero when porosity and water saturation increase. All the three models reduce to the classical Archie equation when the microcrack porosity and clay content are set to 0. It can be seen that the resistivity predicted by the DPCL model is strongly affected by the two properties at low water saturation. The model can be applied at high oil saturation.

Then, the DPCL model is used to analyze the effects of porosity, microcrack porosity, clay content, and water saturation on the electrical properties of tight-oil rocks. Let us consider full water saturation and a clay content of 5%. By adjusting the content of pores and microcracks, the effects of the total and microcrack porosities can be analyzed. Figure 6(a) shows that the resistivity decreases when the two porosities increase. Next, the total and microcrack porosities are set to 10% and 0.05%, respectively, to analyze the influence of clay content and water saturation (Figure 6(b)). The resistivity decreases if these quantities increase, as expected.

*4.2. Elastic Response.* In this case, the properties are as follows. The bulk and shear moduli and density of the frame are 43 GPa, 42 GPa, and 2.65 g/cm$^3$, and those of the clay minerals are 10.5 GPa, 3.5 GPa, and 2.55 g/cm$^3$, respectively. The water bulk modulus is 2.24 GPa, the water density is 1.0016 g/cm$^3$, the oil bulk modulus is 1.27 GPa, and the oil density is 0.79 g/cm$^3$.

Downloaded from http://pubs.geoscienceworld.org/gsa/lithosphere/article-pdf/doi/10.2113/2021/3341849/5355757/3341849.pdf
by OGS Inst Naz Oceanografia Geofisica Sperim - Biblioteca user

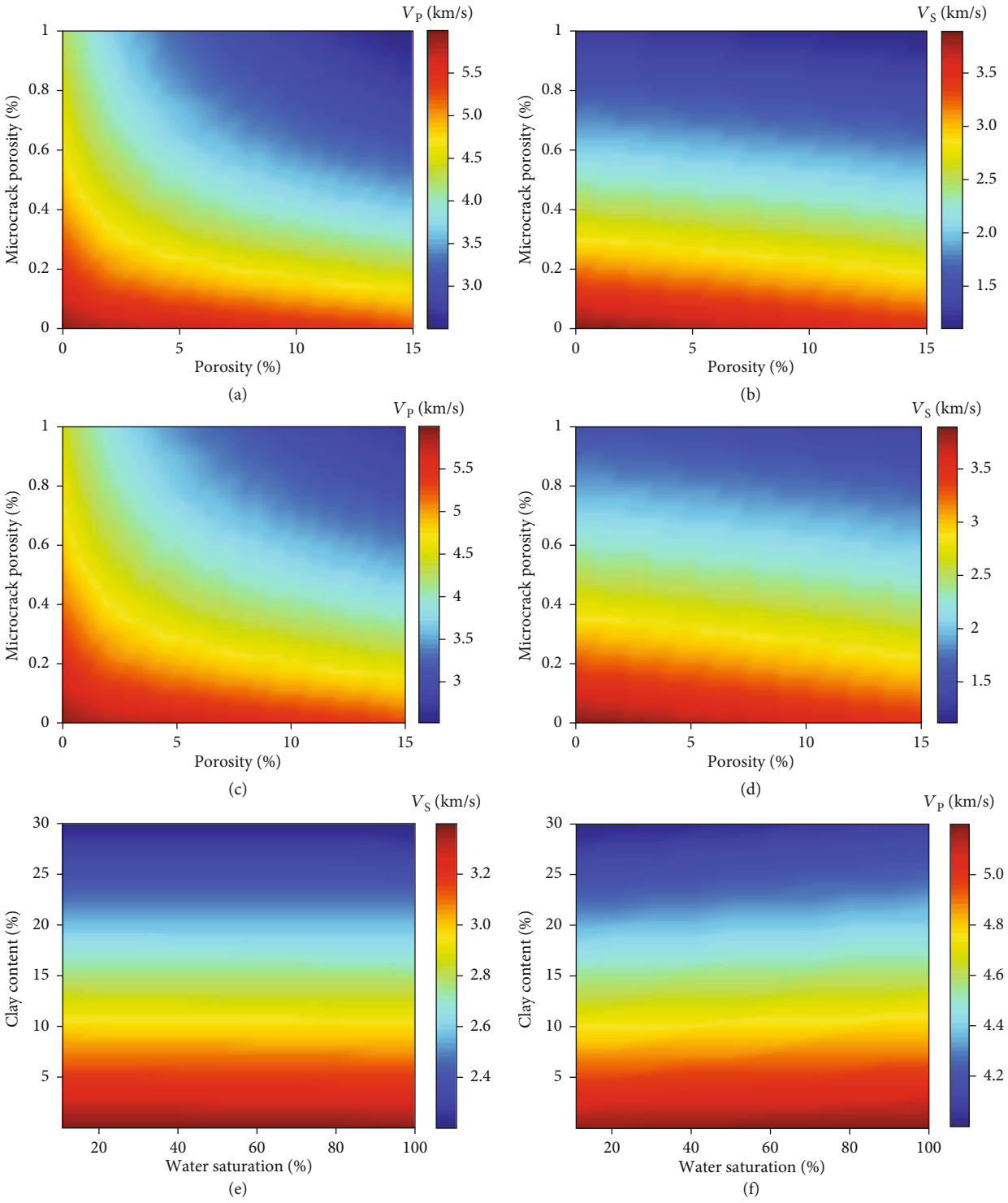


FIGURE 7: P- and S-wave velocities as a function of (a, b) total and microcrack porosities, (c, d) microcrack density and porosity, and (e, f) water saturation and clay content.

We consider full water saturation and clay content of 5% to analyze the effects of the total and microcrack porosities on the elastic wave velocities, as shown in Figures 7(a) and 7(b). Similarly, the relation between microcrack porosity, aspect ratio, and density ([59, 60]) is considered to analyze the effects of microcrack density on the elastic responses (see Figures 7(c) and 7(d)). Then, the total and crack porosities are assumed to be 10% and 0.1%, respectively, and the influence of clay content and water saturation is shown in Figures 7(e) and 7(f). The velocities decrease when both

Downloaded from http://pubs.geoscienceworld.org/gsa/lithosphere/article-pdf/doi/10.2113/2021/3341849/5355757/3341849.pdf
by OGS Inst Naz Oceanografia Geofisica Sperim - Biblioteca user

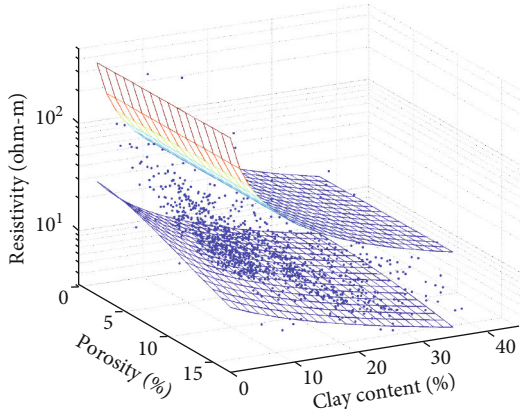


Figure 8: Resistivity as a function of porosity and clay content for the two cases described in Section 4.3 (surfaces). The dots (scatters) represent the data (Well A).

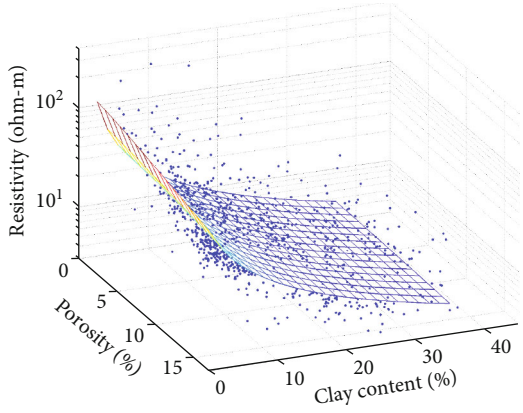


Figure 9: Same as Figure 8, but for the case (details in Section 4.3) where we observe a good match with the data.

porosities and clay content increase and are slightly affected by saturation, with the S-wave velocity almost independent of the type of fluid.

*4.3. Electrical Model and Well-Log Data.* We compare the log data of Well A with the model results. Two cases are considered, namely, high resistivity (full oil saturation): a microcrack porosity of 0.01% and a clay resistivity of 6 ohm-m, and low resistivity (full water saturation): a microcrack porosity of 1% and a clay resistivity of 2 ohm-m. We adjust the porosity and clay content and keep the other parameters constant. Figure 8 shows the resistivity for the two cases (upper and lower surfaces), compared to the log data. As can be seen, resistivity decreases with increasing porosity and clay content, and the data (scatters) are all within the intermediate range between the two cases. Then, we assume an oil saturation of 70%, a clay resistivity of 2 ohm-m, and a microcrack porosity accounting for 5% of total porosity, to match the data, as shown in Figure 9, where the agreement is good. Another set of data (Well B) is selected to verify the DPCL model with the same parameters (Figure 10) and to

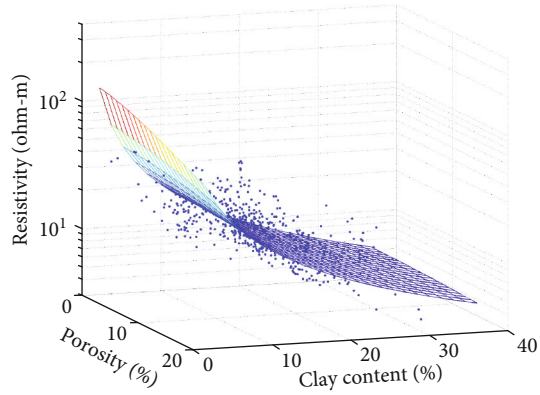


Figure 10: Same as Figure 9, but for Well B.

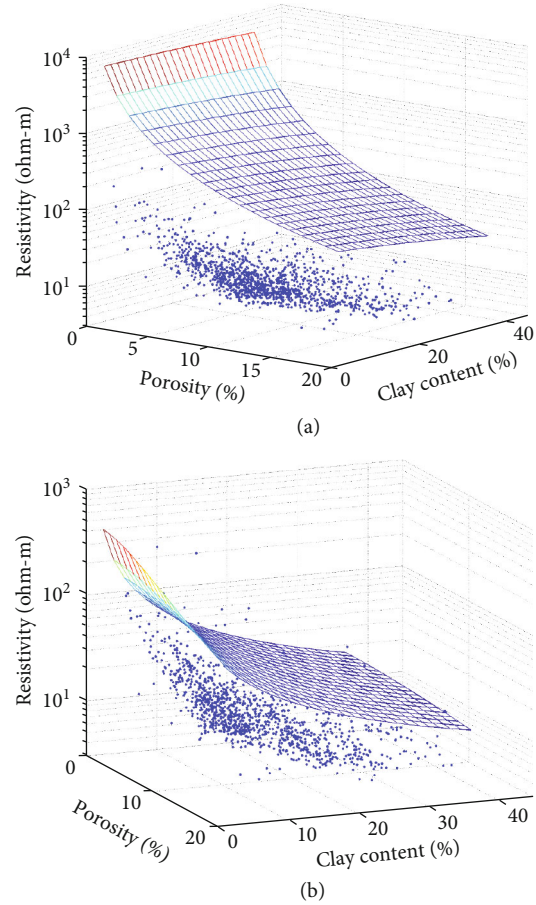


Figure 11: Same as Figure 10, but corresponding to the dual-porosity (a) and Sava & Hardage (b) models.

compare it with the other two electrical models (see Figure 11). The results show that the DPCL model is also consistent with the data of Well B, while the resistivity predicted by the other models is significantly higher.

*4.4. Elastic Model and Well-Log Data.* The experimental data for full oil saturation are compared to the elastic model,

Downloaded from http://pubs.geoscienceworld.org/gsa/lithosphere/article-pdf/doi/10.2113/2021/3341849/5355757/3341849.pdf
by OGS Inst Naz Oceanografia Geofisica Sperim - Biblioteca user

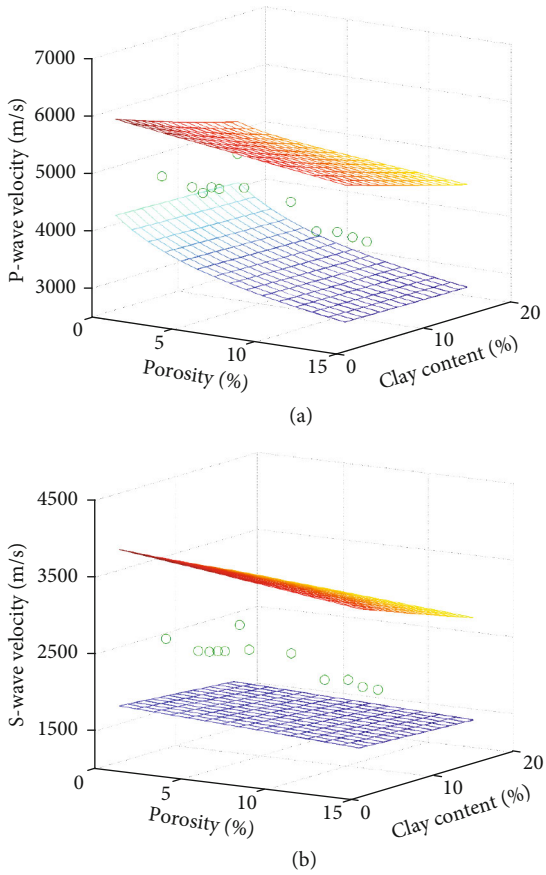


Figure 12: P- (a) and S- (b) wave velocities as a function of porosity and clay content. The ultrasonic data (open circles) and model results at the microcrack porosities of 0.01% (upper surface) and 0.8% (lower surface) are shown.

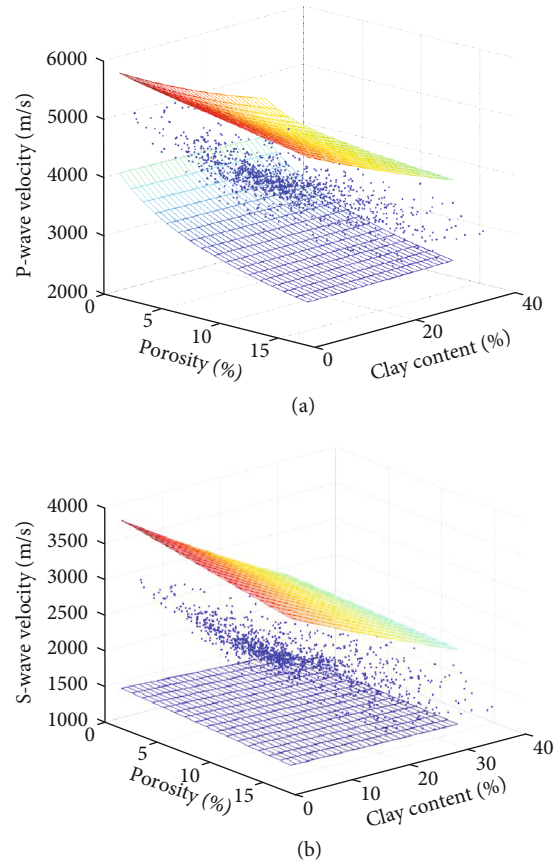


Figure 13: P- (a) and S- (b) wave velocities as a function of porosity and clay content. The log data (dots) and model results at the microcrack porosities of 0.04% (upper surface) and 1% (lower surface) are shown.

where the microcrack porosities are 0.01% and 0.8% (the range of the data). Figure 12 shows the P- and S-wave velocities as a function of porosity and clay content. The velocities decrease with increasing porosity and clay content, which is consistent with the data.

Then, the velocity, porosity, and clay content of Well A are considered. Since the frequencies of the well-log data and ultrasonic are different, there is a difference in velocity (dispersion). Therefore, the model is calibrated with the ultrasonic data and then extrapolated according to the well-log data. According to the reservoir characteristics, we assume 70% oil saturation and microcrack porosities of 0.04% and 1%. The comparison with the log data is shown in Figure 13, where we can see that, similarly to the ultrasonic data, the log (scatters) and model velocities decrease with porosity and clay content.

## 5. Elastic-Electrical Template

*5.1. Set-Up and Calibration.* Next, a 3D elastic-electrical rock-physics template based on resistivity, P-wave impedance, and Poisson's ratio is built. This requires adjusting the total and microcrack porosities and clay content (see the parameters in Table 2). Figure 14 shows the template and log data of Well A. The color bar indicates the porosity (a) and clay content (b), and the black, red, and blue lines are isolines of constant total porosity, microcrack porosity, and clay content, respectively, where the corresponding ranges are given in Table 2. As can be seen, the porosity and clay content of the template are in agreement with the data (scatters). Thus, a quantitative prediction of the reservoir properties can be achieved by overlapping the data on the template.

*5.2. Results.* We superimpose the elastic and electrical attributes on the 3D template and use a grid searching method to estimate the reservoir properties at Wells A and B. These are assigned to the data by minimizing the sum of squares of the differences between the well-log data and the results provided by the template for the three attributes. Figures 15 and 16 show the results and log interpretation results, where total porosity ranges from 3% to 15%, microcrack porosity from 0.2% to 1.2%, and clay content from 5% to 30%. The porosity and clay content curves of the two wells are basically consistent with the predicted curves.

In the actual reports, the producing depth intervals of Wells A and B are mainly at 2105-2200 m and 2250-2300 m

Downloaded from http://pubs.geoscienceworld.org/gsa/lithosphere/article-pdf/doi/10.2113/2021/3341849/5355757/3341849.pdf
by OGS Inst Naz Oceanografia Geofisica Sperim - Biblioteca user

Table 2: Elastic and electrical properties.

| | | | |
|---|---|---|---|
| Matrix bulk modulus ($K_S$) | 43 GPa | Water resistivity ($R_w$) | 0.41 ohm-m |
| Shear modulus ($G_S$) | 42 GPa | Clay resistivity ($R_{sh}$) | 2 ohm-m |
| Density ($\rho_S$) | 2.65 g/cm$^3$ | Lithology coefficient ($a$) | 1 |
| Clay bulk modulus ($K_{sh}$) | 10.5 GPa | Lithology coefficient ($b$) | 1 |
| Shear modulus ($G_{sh}$) | 3.5 GPa | Porosity exponent ($m_0$) | 2 |
| Density ($\rho_{sh}$) | 2.55 g/cm$^3$ | Saturation exponent ($n$) | 2 |
| Water bulk modulus ($K_W$) | 2.24 GPa | Water saturation ($S_W$) | 30% |
| Density ($\rho_W$) | 1.0016 g/cm$^3$ | Total porosity ($\phi$) | 1%-15% |
| Oil bulk modulus ($K_O$) | 1.27 GPa | Microcrack porosity ($\phi_C$) | 0.3%-1.1% |
| Density ($\rho_O$) | 0.79 g/cm$^3$ | Clay content ($V_{sh}$) | 2%-32% |
| Pore aspect ratio | 1 | | |
| Microcrack aspect ratio | 0.002 | | |
| Clay aspect ratio | 0.1 | | |

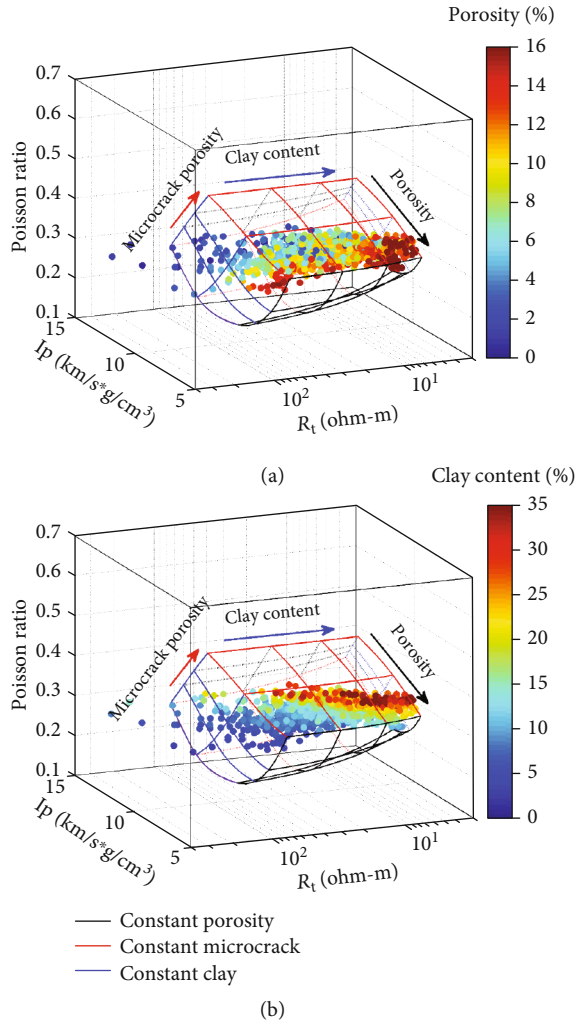


Figure 14: 3D elastic-electrical template and data from Well A, where the color bar represents porosity (a) and clay content (b).

depth, respectively. Compared with Well B, Well A shows higher total and microcrack porosities and lower clay content in the oil production section. Thus, the area where Well A is located has better pore connectivity and higher oil-storage potential. Well A produces 7.39 tons per day and Well B 0.012 tons per day, which are consistent with the predictions.

Downloaded from http://pubs.geoscienceworld.org/gsa/lithosphere/article-pdf/doi/10.2113/2021/3341849/5355757/3341849.pdf
by OGS Inst Naz Oceanografia Geofisica Sperim - Biblioteca user

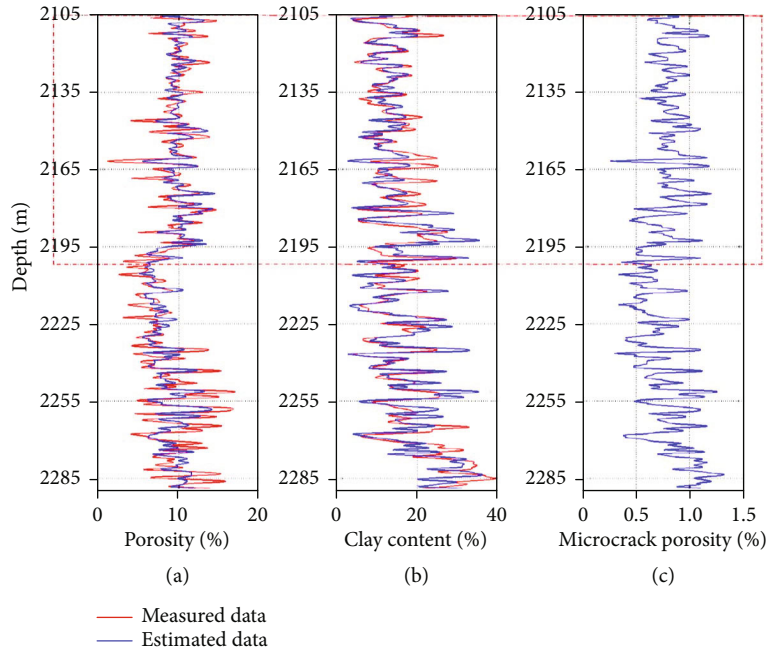


Figure 15: Comparison of the predictions at Well A with the log interpretation results: (a) porosity, (b) clay content, and (c) microcrack porosity. The dotted box indicates the oil production section.

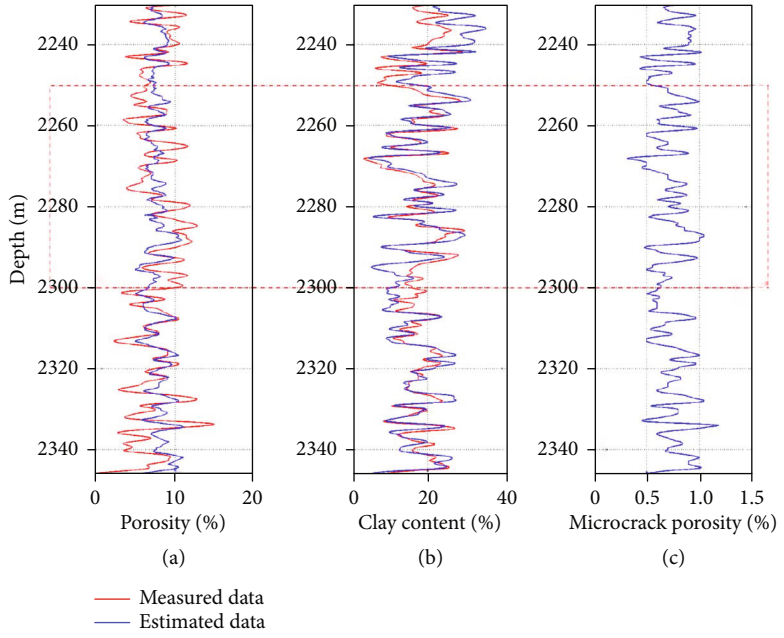


Figure 16: Comparison of the predictions at Well B with the log interpretation results: (a) porosity, (b) clay content, and (c) microcrack porosity. The dotted box indicates the oil production section.

## 6. Conclusions

We have built an elastic/electrical rock-physics template based on electrical resistivity, acoustic impedance, and Poisson's ratio to estimate the properties of tight-oil reservoirs, basically total porosity, microcrack porosity, and clay content. A set of rock samples has been collected and analyzed with scanning electron microscopy and ultrasonic experiments. The gamma-ray value has been used to calculate the clay content, and the resistivity has been obtained as a function of porosity and clay content with a novel dual-porosity model. The results show that high clay content is closely related to high electrical conductivity (or low resistivity), as expected. On the other hand, the Hashin-Shtrikman and differential effective medium equations have been used to establish an elastic model and obtain the P- and S-wave

Downloaded from http://pubs.geoscienceworld.org/gsa/lithosphere/article-pdf/doi/10.2113/2021/3341849/5355757/3341849.pdf
by OGS Inst Naz Oceanografia Geofisica Sperim - Biblioteca user

velocities. Then, the effects of water saturation, total porosity, microcrack porosity, and clay content on wave velocity and resistivity are analyzed, and the results are compared with ultrasonic and well-log data. The presence of pores and microcracks improves the fluid flow properties, while clay content works in the opposite direction.

The template is calibrated with well-log data, and the predictions are compared to log interpretation results and oil production reports of two wells, showing a good agreement. It is shown that the template can effectively be applied to tight-oil reservoirs for the inversion of relevant properties to hydrocarbon exploration.

## Appendix

## A. Clay Volume Estimation

The gamma-ray (Gr) log is used to compute the clay content. The equations are given as [61]

$$\begin{aligned} I_{\mathrm{Gr}} &= \frac{\mathrm{Gr} - \mathrm{Gr}_{\min}}{\mathrm{Gr}_{\max} - \mathrm{Gr}_{\min}}, \\ M_{\mathrm{sh}} &= \frac{2^{\beta * I_{\mathrm{Gr}}} - 1}{2^{\beta} - 1}, \end{aligned} \tag{A.1}$$

where $I_{\mathrm{Gr}}$ is the mud-content index; Gr, $\mathrm{Gr}_{\min}$, and $\mathrm{Gr}_{\max}$ are the natural gamma values of the layer, sandstone, and mudstone, respectively; $M_{\mathrm{sh}}$ is the clay volume, and $\beta$ is the Hirsch index (3.7).

## B. Elastic Model

The bounds for an isotropic linear elastic composite are given by the HS equation [49]

$$\begin{aligned} K^{\mathrm{HS}\pm} &= K_1 + \frac{f_2}{(K_2 - K_1)^{-1} + f_1(K_1 + 4/3\mu_1)}, \\ \mu^{\mathrm{HS}\pm} &= \mu_1 + \frac{f_2}{(\mu_2 - \mu_1)^{-1} + 2f_1(K_1 + 2\mu_1)/[5\mu(K_1 + 4/3\mu_1)]}, \end{aligned} \tag{B.1}$$

where $K_1$ and $K_2$ are the bulk moduli, $\mu_1$ and $\mu_2$ are the shear moduli, and $f_1$ and $f_2$ are the volume fractions of the single phases.

Berryman [50] proposed the following DEM equation for the bulk ($M^*$) and shear ($G^*$) moduli:

$$\begin{aligned} (1-y)\frac{d}{dy}[M^*(y)] &= (M_2 - M^*)Q^{(*2)}(y), \\ (1-y)\frac{d}{dy}[G^*(y)] &= (G_2 - G^*)P^{(*2)}(y), \end{aligned} \tag{B.2}$$

with the initial conditions $M^*(0) = M_1$ and $G^*(0) = G_1$, where $M_1$ and $G_1$ are the bulk and shear moduli of the host material, respectively; $y$ is the content of phase 2; and $M_2$ and $G_2$ are the corresponding moduli. $P$ and $Q$ ([62], p. 3) are geometrical factors.

Wollner and Dvorkin [55] and Monachesi et al. [54] proposed an approximate mixing law to compute the effective fluid modulus $K_f$ based on the arithmetic (Voigt upper bound, $K_{f,\mathrm{AR}}$) and harmonic (Reuss lower bound, $K_{f,\mathrm{HR}}$) averages:

$$\begin{aligned} K_f &= 0.75K_{f,\boldsymbol{AR}} + 0.25K_{f,\boldsymbol{HR}}, \\ K_{f,\boldsymbol{AR}} &= f_1K_{f,1} + f_2K_{f,2}, \\ K_{f,\boldsymbol{HR}} &= \left(\frac{f_1}{K_{f,1}} + \frac{f_2}{K_{f,2}}\right)^{-1}, \end{aligned} \tag{B.3}$$

where $f_1$ and $f_2$ are the water and oil saturations, respectively.

## C. Electrical Model

Aguilera and Aguilera [48] proposed a dual-porosity equation for the fractured reservoirs, such that

$$\frac{1}{R_{\mathrm{t}}} = \frac{1 - \phi_{\mathrm{c}}}{R_0} + \frac{\phi_{\mathrm{c}}}{R_{\boldsymbol{c}}}. \tag{C.1}$$

On the other hand, based on the Archie equation, Sava and Hardage [57] proposed the following clay-bearing electrical equation:

$$\frac{1}{R_{\mathrm{t}}} = \frac{\phi^m S_{\mathrm{w}}^n}{aR_{\mathrm{w}}(1 - V_{\mathrm{sh}})} + \frac{V_{\mathrm{sh}}S_{\mathrm{w}}^{n-1}}{R_{\boldsymbol{sh}}}, \tag{C.2}$$

where the quantities involved are explained in the main text.

## Data Availability

All the relevant data can be accessed by contacting the corresponding author.

## Conflicts of Interest

The authors declare that they have no conflicts of interest.

## Acknowledgments

This work is supported by the National Natural Science Foundation of China (grant no. 41974123), the Postgraduate Research & Practice Innovation Program of Jiangsu Province, the Fundamental Research Funds for the Central Universities, the National Science and Technology Major Project of China (grant no. 2017ZX05069-002), and the Jiangsu Province Science Fund for Distinguished Young Scholars (grant no. BK20200021).

## References

[1] A. Ghanizadeh, C. Clarkson, S. Aquino, O. Ardakani, and H. Sanei, "Petrophysical and geomechanical characteristics of Canadian tight oil and liquid-rich gas reservoirs: I. Pore

Downloaded from http://pubs.geoscienceworld.org/gsa/lithosphere/article-pdf/doi/10.2113/2021/3341849/5355757/3341849.pdf
by OGS Inst Naz Oceanografia Geofisica Sperim - Biblioteca user

network and permeability characterization," *Fuel*, vol. 153, pp. 664–681, 2015.

[2] C. Li, H. Wang, L. Wang, Y. Kang, K. Hu, and Y. Zhu, "Characteristics of tight oil sandstone reservoirs: a case study from the Upper Triassic Chang 7 Member in Zhenyuan area, Ordos Basin, China," *Arabian Journal of Geosciences*, vol. 13, no. 2, p. 78, 2020.

[3] Y. Wang, J. Cao, K. Tao, E. Li, C. Ma, and C. Shi, "Reevaluating the source and accumulation of tight oil in the middle Permian Lucaogou Formation of the Junggar Basin, China," *Marine and Petroleum Geology*, vol. 117, article 104384, 2020.

[4] W. Yan, J. Sun, N. Golsanami et al., "Evaluation of wettabilities and pores in tight oil reservoirs by a new experimental design," *Fuel*, vol. 252, pp. 272–280, 2019.

[5] M. Lu, H. Cao, W. Sun et al., "Quantitative prediction of seismic rock physics of hybrid tight oil reservoirs of the Permian Lucaogou Formation, Junggar Basin, Northwest China," *Journal of Asian Earth Sciences*, vol. 178, pp. 216–223, 2019.

[6] H. Sun, L. Duan, L. Liu et al., "The influence of micro-fractures on the flow in tight oil reservoirs based on pore-network models," *Energies*, vol. 12, no. 21, p. 4104, 2019.

[7] D. Zheng, X. Pang, L. Zhou et al., "Critical conditions of tight oil charging and determination of the lower limits of petrophysical properties for effective tight reservoirs: a case study from the Fengcheng Formation in the Fengcheng area, Junggar Basin," *Journal of Petroleum Science and Engineering*, vol. 190, article 107135, 2020.

[8] M. Benaafi, M. Hariri, G. Bertotti, A. Al-Shaibani, O. Abdullatif, and M. Makkawi, "Natural fracture system of the Cambro-Permian Wajid Group, Wadi Al-Dawasir, SW Saudi Arabia," *Journal of Petroleum Science and Engineering*, vol. 175, pp. 140–158, 2019.

[9] R. Nelson, *Geologic Analysis of Naturally Fractured Reservoirs*, Elsevier, 2001.

[10] M. Pang, J. Ba, J. Carcione, S. Picotti, J. Zhou, and R. Jiang, "Estimation of porosity and fluid saturation in carbonates from rock-physics templates based on seismicQ," *Geophysics*, vol. 84, no. 6, pp. M25–M36, 2019.

[11] M. Pang, J. Ba, L. Fu, J. Carcione, U. Markus, and L. Zhang, "Estimation of microfracture porosity in deep carbonate reservoirs based on 3D rock-physics templates," *Interpretation*, vol. 8, no. 4, pp. SP43–SP52, 2020.

[12] C. Fang, B. Pan, Y. Wang, Y. Rao, Y. Guo, and J. Li, "Pore-scale fluid distributions determined by nuclear magnetic resonance spectra of partially saturated sandstones," *Geophysics*, vol. 84, no. 3, pp. MR107–MR114, 2019.

[13] Q. Gan, D. Xu, J. Tang, and Y. Wang, "Seismic resolution enhancement for tight-sand gas reservoir characterization," *Journal of Geophysics and Engineering*, vol. 6, no. 1, pp. 21–28, 2009.

[14] J. Hu, R. Sun, and Y. Zhang, "Investigating the horizontal well performance under the combination of micro-fractures and dynamic capillary pressure in tight oil reservoirs," *Fuel*, vol. 269, article 117375, 2020.

[15] Y. Sun, Q. Wu, M. Wei, B. Bai, and Y. Ma, "Experimental study of friction reducer flows in microfracture," *Fuel*, vol. 131, pp. 28–35, 2014.

[16] L. Zhao, C. Cao, Q. Yao et al., "Gassmann consistency for different inclusion-based effective medium theories: implications for elastic interactions and poroelasticity," *Journal of Geophysical Research: Solid Earth*, vol. 125, no. 3, article e2019JB018328, 2020.

[17] L. Zhao, X. Qin, D. Han, J. Geng, Z. Yang, and H. Cao, "Rock-physics modeling for the elastic properties of organic shale at different maturity stages," *Geophysics*, vol. 81, no. 5, pp. D527–D541, 2016.

[18] L. Zhao, Q. Yao, D. Han, F. Yan, and M. Nasser, "Characterizing the effect of elastic interactions on the effective elastic properties of porous, cracked rocks," *Geophysical Prospecting*, vol. 64, no. 1, pp. 157–169, 2016.

[19] M. Pang, J. Ba, and J. M. Carcione, "Characterization of gas saturation in tight-sandstone reservoirs with rock-physics templates based on seismic Q," *Journal of Energy Engineering*, vol. 147, no. 3, article 04021011, 2021.

[20] M. Pang, J. Ba, J. M. Carcione, L. Zhang, R. Ma, and Y. Wei, "Seismic identification of tight-oil reservoirs by using 3D rock-physics templates," *Journal of Petroleum Science and Engineering*, vol. 201, article 108476, 2021.

[21] K. Xi, Y. Cao, K. Liu et al., "Authigenic minerals related to wettability and their impacts on oil accumulation in tight sandstone reservoirs: an example from the Lower Cretaceous Quantou Formation in the southern Songliao Basin, China," *Journal of Asian Earth Sciences*, vol. 178, pp. 173–192, 2019.

[22] P. H. Nelson, "Pore-throat sizes in sandstones, tight sandstones, and shales," *AAPG Bulletin*, vol. 93, no. 3, pp. 329–340, 2009.

[23] T. Stroker, N. Harris, W. Elliott, and J. Wampler, "Diagenesis of a tight gas sand reservoir: Upper Cretaceous Mesaverde Group, Piceance Basin, Colorado," *Marine and Petroleum Geology*, vol. 40, pp. 48–68, 2013.

[24] D. Xiao, S. Jiang, D. Thul, S. Lu, L. Zhang, and B. Li, "Impacts of clay on pore structure, storage and percolation of tight sandstones from the Songliao Basin, China: implications for genetic classification of tight sandstone reservoirs," *Fuel*, vol. 211, pp. 390–404, 2018.

[25] J. Ba, R. Ma, J. Carcione, and S. Picotti, "Ultrasonic wave attenuation dependence on saturation in tight oil siltstones," *Journal of Petroleum Science and Engineering*, vol. 179, pp. 1114–1122, 2019.

[26] J. Ba, W. Xu, L. Fu, J. Carcione, and L. Zhang, "Rock anelasticity due to patchy saturation and fabric heterogeneity: a double double-porosity model of wave propagation," *Solid Earth*, vol. 122, no. 3, pp. 1949–1976, 2017.

[27] R. Ma, J. Ba, J. Carcione, X. Zhou, and F. Li, "Dispersion and attenuation of compressional waves in tight oil reservoirs: experiments and simulations," *Applied Geophysics*, vol. 16, no. 1, pp. 33–45, 2019.

[28] R. Ma and J. Ba, "Coda and intrinsic attenuations from ultrasonic measurements in tight siltstones," *Journal of Geophysical Research*, vol. 125, no. 4, 2020.

[29] W. Tan, J. Ba, T. Muller, G. Fang, and H. Zhao, "Rock physics model of tight oil siltstone for seismic prediction of brittleness," *Geophysical Prospecting*, vol. 68, no. 5, pp. 1554–1574, 2020.

[30] H. Pan, Y. Zhang, H. Li, T. Liu, J. Deng, and Y. Zhao, "Joint inversion of elastic-electrical data for gas hydrate reservoirs based on Bayesian theory," *OGP*, vol. 53, no. 3, pp. 568–577, 2018.

[31] P. Cilli and M. Chapman, "Modelling the elastic and electrical proper-ties of rocks with complex pore geometries," in *80th EAGE Annual International Conference and Exhibition*, Copenhagen, Denmark, June 2018.

Downloaded from http://pubs.geoscienceworld.org/gsa/lithosphere/article-pdf/doi/10.2113/2021/3341849/5355757/3341849.pdf
by OGS Inst Naz Oceanografia Geofisica Sperim - Biblioteca user

[32] P. Cilli and M. Chapman, "The power-law relation between inclusion aspect ratio and porosity: implications for electrical and elastic modeling," *Journal of Geophysical Research: Solid Earth*, vol. 125, no. 5, pp. 1–25, 2020.

[33] A. Gabàs, A. Macau, B. Benjumea et al., "Joint audio-magnetotelluric and passive seismic imaging of the Cerdanya Basin," *Surveys in Geophysics*, vol. 37, no. 5, pp. 897–921, 2016.

[34] T. Han, A. Best, J. Sothcott, and L. MacGregor, "Pressure effects on the joint elastic-electrical properties of reservoir sandstones," *Geophysical Prospecting*, vol. 59, no. 3, pp. 506–517, 2011.

[35] T. Han, S. Liu, D. Xu, and L. Fu, "Pressure-dependent cross-property relationships between elastic and electrical properties of partially saturated porous sandstones," *Geophysics*, vol. 85, no. 3, pp. MR107–MR115, 2020.

[36] T. Han, Z. Wei, and F. Li, "How the effective pore and grain shapes are correlated in Berea sandstones: implications for joint elastic-electrical modeling," *Geophysics*, vol. 85, no. 3, pp. MR147–MR154, 2020.

[37] E. H. Jensen, L. J. Gelius, T. A. Johansen, and Z. Wang, "Consistent joint elastic-electrical differential effective-medium modelling of compacting reservoir sandstones," *Geophysical Prospecting*, vol. 61, no. 4, pp. 788–802, 2013.

[38] J. M. Carcione, B. Ursin, and J. I. Nordskag, "Cross-property relations between electrical conductivity and the seismic velocity of rocks," *Geophysics*, vol. 72, no. 5, pp. E193–E204, 2007.

[39] T. Han, M. Clennell, A. Cheng, and M. Pervukhina, "Are self-consistent models capable of jointly modeling elastic velocity and elec-trical conductivity of reservoir sandstones?," *Geophysics*, vol. 81, no. 4, pp. D377–D382, 2016.

[40] H. Pan, H. Li, D. Grana, Y. Zhang, T. Liu, and C. Geng, "Quantitative characterization of gas hydrate bearing sediment using elastic-electrical rock physics models," *Marine and Petroleum Geology*, vol. 105, pp. 273–283, 2019.

[41] E. Kazatchenko, M. Markov, and A. Mousatov, "Joint modeling of acoustic velocities and electrical conductivity from unified microstructure of rocks," *Journal of Geophysical Research*, vol. 109, no. B1, article B01202, 2004.

[42] T. Han, A. Best, J. Sothcott, and L. MacGregor, "Joint elastic-electrical properties of reservoir sandstones and their relationships with petrophysical parameters," *Geophysical Prospecting*, vol. 59, no. 3, pp. 518–535, 2011.

[43] J. M. Carcione, G. Seriani, and D. Gei, "Acoustic and electromagnetic properties of soils saturated with salt water and NAPL," *Journal of Applied Geophysics*, vol. 52, no. 4, pp. 177–191, 2003.

[44] J. M. Carcione, D. Gei, S. Picotti, and A. Michelini, "Cross-hole electromagnetic and seismic modeling for CO2 detection and monitoring in a saline aquifer," *Journal of Petroleum Science and Engineering*, vol. 100, pp. 162–172, 2012.

[45] M. Lee, "Connectivity equation and shaly-sand correction for electrical resistivity," U.S. Geological Survey, Scientific Investigations Report 2011-5005, 2011.

[46] C. Peng, C. Zou, Z. Lu et al., "Characteristics of gas hydrate reservoirs and their effect on petrophysical properties in the Muli area, Qinghai-Tibetan plateau permafrost," *Journal of Natural Gas Science and Engineering*, vol. 57, pp. 266–283, 2018.

[47] L. Dewitte, "Relation between resisitivities and fluid content of porous rock," *Oil and Gas*, vol. 49, no. 8, pp. 120–132, 1950.

[48] M. S. Aguilera and R. Aguilera, "Improved models for petrophysical analysis of dual porosity reservoirs," *Petrophysics*, vol. 44, no. 1, 2003.

[49] Z. Hashin and S. Shtrikman, "A variational approach to the theory of the elastic behaviour of multiphase materials," *Journal of the Mechanics and Physics of Solids*, vol. 11, no. 2, pp. 127–140, 1963.

[50] J. G. Berryman, "Single-scattering approximations for coefficients in Biot's equations of poroelasticity," *Acoustical Society of America Journal*, vol. 91, no. 2, pp. 551–571, 1992.

[51] F. Gassmann, "Über die Elastizität poröser Medien," *Vierteljahrsschrift der naturforschenden Gesellschaft in Zürich*, vol. 96, pp. 1–23, 1951.

[52] L. Shi, Z. Wang, G. Zhang, Y. Zhang, and E. Xing, "Distribution and formation of tight oil in Qijia area, Songliao Basin, NE China," *Petroleum Exploration and Development*, vol. 42, no. 1, pp. 48–55, 2015.

[53] M. Batzle and Z. Wang, "Seismic properties of pore fluids," *Geophysics*, vol. 57, no. 11, pp. 1396–1408, 1992.

[54] L. Monachesi, U. Wollner, and J. Dvorkin, "Effective pore fluid bulk modulus at patchy saturation: an analytic study," *Journal of Geophysical Research: Solid Earth*, vol. 125, no. 1, 2020.

[55] U. Wollner and J. Dvorkin, "Effective bulk modulus of the pore fluid at patchy saturation," *Geophysical Prospecting*, vol. 66, no. 7, pp. 1372–1383, 2018.

[56] G. E. Archie, "The electrical resistivity log as an aid in determining some reservoir characteristics," *Transactions of the AIME*, vol. 146, no. 1, pp. 54–62, 1942.

[57] D. Sava and B. Hardage, "Gas-hydrate concentration and uncertainty estimation from electrical-resistivity logs: examples from Green Canyon, Gulf of Mexico," in *77th SEG Technical Program Expanded Abstracts*, pp. 1579–1583, Society of Exploration Geophysicists, San Antonio, USA, 2007.

[58] W. Z. W. Bakar, I. M. Saaid, M. R. Ahmad, Z. Amir, and S. Q. A. Mahat, "Derivation of formation factor in shaly sandstone with geometry and clay conductivity effects," *Journal of Petroleum Science and Engineering*, vol. 182, article 106359, 2019.

[59] J. A. Hudson, "Wave speeds and attenuation of elastic waves in material containing cracks," *Geophysical Journal International*, vol. 64, no. 1, pp. 133–150, 1981.

[60] L. Zhao, M. Nasser, and D. Han, "Quantitative geophysical pore-type characterization and its geological implication in carbonate reservoirs," *Geophysical Prospecting*, vol. 61, no. 4, pp. 827–841, 2013.

[61] Z. Li, *Processing and Comprehensive Interpretation of Geophysical Well-Logging Data*, Beijing Geological Publisher, 2018.

[62] J. G. Berryman, "Long-wavelength propagation in composite elastic media," *Journal of Acoustical Society of America*, vol. 68, no. 6, pp. 1809–1831, 1980.

Downloaded from http://pubs.geoscienceworld.org/gsa/lithosphere/article-pdf/doi/10.2113/2021/3341849/5355757/3341849.pdf
by OGS Inst Naz Oceanografia Geofisica Sperim - Biblioteca user